ISSN 2176-5480

22nd International Congress of Mechanical Engineering (COBEM 2013)
November 3-7, 2013, Ribeirão Preto, SP, Brazil

HEAT TRANSFER ENHANCEMENT THROUGH GOERTLER VORTICES

Vinicius Malatesta
Leandro Franco de Souza
Laboratory of Applied Mathematics and Sientific Computing, Departament of Applied Mathematics and Statistics, ICMC - University of Sao Paulo, Sao Carlos, Sao Paulo, Brazil
malatest@icmc.usp.br; lefraso@icmc.usp.br

Joseph T. C. Liu
School of Engineering and Center for Fluid Mechanics, Brown University, Providence, Rhode Island, USA
Joseph_Liu@brown.edu

Abstract. *The centrifugal instability mechanism in boundary layers flows over concave surfaces is responsible for the development of streamwise counter-rotating vortices, known as Goertler vortices. These Vortices create two regions in the spanwise direction, the upwash and downwash regions. The downwash region is responsible to compress the boundary layer towards the wall, increasing drag and heat transfer rates. The upwash region does the opposite. In the nonlinear region the downwash region becomes wider than the upwash region. In the present paper, the influence of the Goertler vortices spanwise wavelength in the heat transfer enhancement is studied numerically, the Stanton number was used to verify the relation between the vortex wavelength and the wall heat transfer. The results show that steady Goertler flow can reach heat transfer rates higher than the turbulent values, even without reaching secondary instability region.*

Keywords: *Centrifugal instability, Goertler vortices, Heat transfer rates, Spatial direct numerical simulation*

1. INTRODUCTION

A large amount of research has been concerned with streamwise vortices in boundary layer flows with heat transfer. Different aaproaches were adopted, for examples the theoretical (Saffmann, 1992) and computational study (Liu and Lee, 1995) on Goertler vortices. The practical interest in intensifying surface heat transfer rates with the least penalty follows the need to reduce energy consumption via more efficient systems. Fiebig (1996) studied streamwise vortices and heat transfer, where he analyzed the influence of vortices on heat transfer in boundary layers flows. The vortex generation in his work was done via winglets. The vortex generators of winglet type cause a great loss in the system because, although it can double the rate of heat transfer, it almost quadruples the drag. Fiebig (1996) suggested that the longitudinal vortices are more effective than the transverse vortices for heat transfer enhancement and transverse vortices lead to oscillations and transition to turbulence with lower Reynolds numbers than the longitudinal vortices.

Mitsudharmadi *et al.* (2004) conducted a study in a boundary layer over a concave wall in the presence of forced wavelength Goertler (streamwise) vortices. The mean velocity contours in y-z plane demonstrates that the nonlinear region of the vortices in which the boundary-layer flow is dominated by the mushroom-like structures.

The Goertler vortices are responsible for generating strong distortions in the velocity profiles (Liu and Lee, 1995). As the vortices are counter-rotating, two regions arise between them: upwash and downwash regions. When the vortices amplitude is high, in the non-linear development region, a mushroom-type structure, with the streamwise velocity distribution in a crosscut plane is formed. This new velocity distribution differs from the Blasius boundary layer. Therefore, taking into account the thermal boundary layer, an spanwise–average increase in the heat transfer is observed.

Liu (2008) carried out studies to explain theoretically the rate of heat transfer in aboundary layer flow over a slightly concave surface. He concluded that one can greatly enhance the heat transfer, paying the price of almost one to one in drag. Some experimental studies were conducted showing that the enhancement in heat transfer in Goertler flow can be higher than the one observed in turbulent flows (Peerhossaini, 1987).

A parabolized formulation was adopted by Liu and Lee (1995) to study the influence on the Prandtl number in the heat transfer rates of boundary layer flows over a concave wall. They studied flows with 3 different Prandtl numbers ($Pr = 0.72, 1.0$ and 7.07). The spanwise wavenumber was the same that Swearingen and Blackwelder (1987). Their results shows that one can achieve high gains in heat transfer rates with the presence of Goertler vortices.

Momayez and Peershossaini (2004) and Momayez *et al.* (2004) conducted experiments where conditions were carried out on concave surface with heat transfer in order to understand the effects of Goertler vortices and its transition to turbulence on heat transfer from the wall to the boundary layer. The experiments were run at nominal freestream velocities of $U_n = 2, 3, 4.8, 7$, and $9ms^{-1}$ and the for wavelengths values of $\lambda = 2.5, 5, 10, 15, 20, 25, 30mm$. They concluded that Goertler number predicts satisfactorily the different stages of Goertler stability, first primary Goertler instability appears for $G \geq 3.5$, heat transfer reaches the turbulent level with values for $G \geq 6.5$, the secondary instability and transition to turbulence is accomplished for $G \geq 9$. They divided the evolution of the Stanton number in three regions: the first region

ISSN 2176-5480

the heat transfer on the concave wall deviates gradually from the flat plate; the second region the heat transfer coefficient gradually reaches values close to or above the turbulent boundary layer values on a flat plate; and the third region the heat transfer ceases to increase and follows the flat-plate turbulent curve. The authors say that, in the last region, the secondary instability grows rapidly and induces a premature transition to turbulence.

Other experiments were done in a similar way (Tandiano *et al.*, 2009), where it was studied the development of wall shear layer stress in concave surface boundary layer flow in the presence of Goertler vortices. They analyzed the flow by hot-wire measurements, and vertical perturbation wires were adopted to introduce perturbations in a selected wavelength. The author concludes that the spanwise-averaged wall shear stress coefficient C_f, which initially follows the Blasius curve, increases well above the local turbulent boundary layer value further downstream due to the nonlinear effects of Goertler instability and to the secondary instabilities.

The cross-sectional heat advection distribution obtained with Goertler flow is very different from the laminar boundary layer on a flat surface. According to linear theory, the boundary layer flow over a concave wall becomes unstable at some critical Goertler number (Floryan and Saric, 1982) and its linear amplification occurs. The first effect of Goertler vortices in the wall heat transfer thus appears in its nonlinear development. Momayez *et al.* (2009) show that the intensification of heat transfer is related to the growth of Goertler vortices under the effect of centrifugal instability and to secondary instabilities.

In Girgis and Liu (2006), the spanwise–averaged streamwise-velocity gradient, obtained by Goertler flow, is studied in terms of skin friction. The skin friction due to nonlinear steady longitudinal Goertler vortex can already nearly bridge the transition from the local laminar skin friction to turbulent skin friction values. Their results were based in the experimental measurements (Swearingen and Blackwelder, 1987). The emphasis is placed on the nonlinear modification of the steady problem by Reynolds stresses of the wavy disturbance, and it is found that skin friction increases well above the turbulent boundary layer value.

In the present paper it is studied numerically the influence of the Goertler vortices spanwise wavelength in heat transfer enhancement, the Stanton number was used to verify the relation between the vortex wavelength and the wall heat transfer. A simulation code was developed and implemented using Spatial Direct Numerical Simulation (SDNS). The studies focused in the same parameters studied in (Momayez and Peershossaini, 2004) and (Momayez *et al.*, 2004). Disturbances were introduced with the same amplitude for six different spanwise wavelengths, namely: $\lambda_z = 0.05, \lambda_z = 0.10, \lambda_z = 0.15, \lambda_z = 0.20, \lambda_z = 0.25$ and $\lambda_z = 0.30$. The Prandtl number adopted was $Pr = 0.72$.

2. Formulation

In this section the governing equations and the numerical methodology are presented. The Navier-Stokes equations, written in the vorticity-velocity formulation, were discretized using high-order finite-differences and spectral approximations for the spatial derivatives. A fourth order Runge-Kutta scheme was adopted for the temporal discretization.

2.1 Governing Equations

The governing equations are the incompressible equations with constant viscosity for a Newtonian fluid. Defining the vorticity as the negative curl of the velocity vector, and using the fact that both the velocity and the vorticity fields are solenoidal, one can obtain the following vorticity transport equation in each direction:

$$\frac{\partial \widetilde{\omega}_x}{\partial t} + \frac{\partial \widetilde{a}}{\partial y} - \frac{\partial \widetilde{b}}{\partial z} + \frac{Go^2}{\sqrt{Re}}\frac{\partial \widetilde{d}}{\partial z} = \frac{1}{Re}\nabla^2 \widetilde{\omega}_x, \tag{1}$$

$$\frac{\partial \widetilde{\omega}_y}{\partial t} + \frac{\partial \widetilde{c}}{\partial z} - \frac{\partial \widetilde{a}}{\partial x} = \frac{1}{Re}\nabla^2 \widetilde{\omega}_y, \tag{2}$$

$$\frac{\partial \widetilde{\omega}_z}{\partial t} + \frac{\partial \widetilde{b}}{\partial x} - \frac{\partial \widetilde{c}}{\partial y} - \frac{Go^2}{\sqrt{Re}}\frac{\partial \widetilde{d}}{\partial x} = \frac{1}{Re}\nabla^2 \widetilde{\omega}_z, \tag{3}$$

where

$$\widetilde{a} = \widetilde{\omega}_x \widetilde{v} - \widetilde{\omega}_y \widetilde{u}, \tag{4}$$

$$\widetilde{b} = \widetilde{\omega}_z \widetilde{u} - \widetilde{\omega}_x \widetilde{w}, \tag{5}$$

$$\widetilde{c} = \widetilde{\omega}_y \widetilde{w} - \widetilde{\omega}_z \widetilde{v}, \tag{6}$$

$$\widetilde{d} = \widetilde{u}^2, \tag{7}$$

ISSN 2176-5480

are the nonlinear terms resulting from convection, vortex stretching and vortex bending. The variables $(\widetilde{u}, \widetilde{v}, \widetilde{w}, \widetilde{\omega}_x, \widetilde{\omega}_y, \widetilde{\omega}_z)$ are the velocity and vorticity components in the streamwise, wall-normal and spanwise directions respectively; $\widetilde{t}$ is the time. The Laplace operator is:

$$\nabla^2 = \left(\frac{\partial^2}{\partial x^2} + \frac{\partial^2}{\partial y^2} + \frac{\partial^2}{\partial z^2} \right). \tag{8}$$

The continuity equation is given by:

$$\frac{\partial \widetilde{u}}{\partial x} + \frac{\partial \widetilde{v}}{\partial y} + \frac{\partial \widetilde{w}}{\partial z} = 0. \tag{9}$$

The heat transfer transport equation adopted in the present work is:

$$\frac{\partial \widetilde{\theta}}{\partial t} + \frac{\partial \widetilde{u}\widetilde{\theta}}{\partial x} + \frac{\partial \widetilde{v}\widetilde{\theta}}{\partial y} + \frac{\partial \widetilde{w}\widetilde{\theta}}{\partial z} = \frac{1}{Re\, Pr} \nabla^2 \widetilde{\theta}, \tag{10}$$

where $\widetilde{\theta}$ is the non dimensional temperature given by $\widetilde{\theta} = (T - T_0)/(T_\infty - T_0)$, where T is the dimensional temperature, and T_∞ and T_0 are the temperature values outside from the thermal boundary layer and at the wall, respectively.

The above equations are presented in a non-dimensional form. The reference length is a plate characteristic length L and the reference velocity is the free stream velocity U_∞. The Reynolds number is given by $Re = U_\infty L/\nu$, where ν is the kinematic viscosity. The Prandtl number is given by $Pr = \nu/\alpha$, where ν is the kinematic viscosity and α is the thermal diffusivity of the fluid. The Goertler number is given by $Go = (k_c\sqrt{Re})^{1/2}$. The terms $Go^2 \frac{\partial \widetilde{d}}{\partial x}/(\sqrt{Re})$ and $Go^2 \frac{\partial \widetilde{d}}{\partial z}/(\sqrt{Re})$ are the leading order curvature terms, where $h = 1 - k_c y$, $k_c = L/R$ is the wall curvature and R is the curvature radius. The objective of the current study is on the Goertler flow, therefore the simulations were performed with the introduction of steady disturbances only.

Taking the definition of the vorticity and the mass conservation equation, one can obtain Poisson-type equations for each velocity component:

$$\frac{\partial^2 \widetilde{u}}{\partial x^2} + \frac{\partial^2 \widetilde{u}}{\partial z^2} = -\frac{\partial \widetilde{\omega}_y}{\partial z} - \frac{\partial^2 \widetilde{v}}{\partial x \partial y}, \tag{11}$$

$$\frac{\partial^2 \widetilde{v}}{\partial x^2} + \frac{\partial^2 \widetilde{v}}{\partial y^2} + \frac{\partial^2 \widetilde{v}}{\partial z^2} = -\frac{\partial \widetilde{\omega}_z}{\partial x} + \frac{\partial \widetilde{\omega}_x}{\partial z}, \tag{12}$$

$$\frac{\partial^2 \widetilde{w}}{\partial x^2} + \frac{\partial^2 \widetilde{w}}{\partial z^2} = \frac{\partial \widetilde{\omega}_y}{\partial x} - \frac{\partial^2 \widetilde{v}}{\partial y \partial z}. \tag{13}$$

2.2 Disturbance Formulation

A disturbance formulation was adopted in the current study, therefore the flow variables were decomposed in a base flow and a perturbation:

$$\widetilde{f} = f_b + f, \tag{14}$$

where $\widetilde{f} = \{\widetilde{u}, \widetilde{v}, \widetilde{w}, \widetilde{\omega}_x, \widetilde{\omega}_y, \widetilde{\omega}_z, \widetilde{\Theta}\}$ are the total flow variables. The base flow is considered two-dimensional, therefore only u_b, v_b, ω_{z_b} and θ_b are taken into account, where the index b indicates the base flow.

With such formulation, the stability analysis of any base flow (Blasius, Falkner-Skan, etc.), can be easily performed as the linear and nonlinear terms can be isolated. Some disadvantages of this formulation are the indirect access to the flow variables and a higher memory usage due to the larger number of variables.

Introducing Eq. (14) in the equations (1) – (3), (10) – (13) and subtracting the base quantities, the equations for the perturbations result in:

$$\frac{\partial \omega_x}{\partial t} + \frac{\partial a}{\partial y} - \frac{\partial b}{\partial z} + \frac{Go^2}{\sqrt{Re}} \frac{\partial d}{\partial z} = \frac{1}{Re} \nabla^2 \omega_x, \tag{15}$$

$$\frac{\partial \omega_y}{\partial t} + \frac{\partial c}{\partial z} - \frac{\partial a}{\partial x} = \frac{1}{Re} \nabla^2 \omega_y, \tag{16}$$

$$\frac{\partial \omega_z}{\partial t} + \frac{\partial b}{\partial x} - \frac{\partial c}{\partial y} - \frac{Go^2}{\sqrt{Re}} \frac{\partial d}{\partial x} = \frac{1}{Re} \nabla^2 \omega_z, \tag{17}$$

ISSN 2176-5480

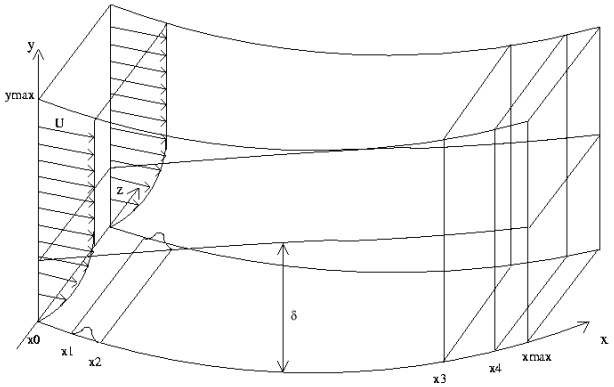

Figure 1: Computational Domain.

$$\frac{\partial^2 u}{\partial x^2} + \frac{\partial^2 u}{\partial z^2} = -\frac{\partial \omega_y}{\partial z} - \frac{\partial^2 v}{\partial x \partial y}, \tag{18}$$

$$\frac{\partial^2 v}{\partial x^2} + \frac{\partial^2 v}{\partial y^2} + \frac{\partial^2 v}{\partial z^2} = -\frac{\partial \omega_z}{\partial x} + \frac{\partial \omega_x}{\partial z}, \tag{19}$$

$$\frac{\partial^2 w}{\partial x^2} + \frac{\partial^2 w}{\partial z^2} = \frac{\partial \omega_y}{\partial x} - \frac{\partial^2 v}{\partial y \partial z}, \tag{20}$$

$$\frac{\partial \theta}{\partial t} + \frac{\partial e}{\partial x} + \frac{\partial f}{\partial y} + \frac{\partial g}{\partial z} = \frac{1}{Re\ Pr}\nabla^2 \theta, \tag{21}$$

where the nonlinear terms a, b, c, d, e and g are:

$$a = \omega_x(v_b + v) - \omega_y(u_b + u), \tag{22}$$

$$b = (\omega_{z_b} + \omega_z)(u_b + u) - \omega_x w, \tag{23}$$

$$c = \omega_y w - (\omega_{z_b} + \omega_z)(v_b + v), \tag{24}$$

$$d = 2u_b u + u^2. \tag{25}$$

$$e = u_b\theta + u\theta_b + u\theta, \tag{26}$$

$$f = v_b\theta + v\theta_b + v\theta, \tag{27}$$

$$g = w(\theta_b + \theta). \tag{28}$$

3. Numerical Method

In this section the discretization of the adopted equations and the boundary conditions adopted in the simulations are shown. The computational domain is illustrated in Fig. 1.

3.1 Spectral Aproximation

The flow is assumed to be periodic in the spanwise direction. Therefore, the flow field can be expanded in Fourier series with K spanwise Fourier modes:

$$f(x, y, z, t) = \sum_{k=0}^{K} F_k(x, y, t) e^{(i\beta_k z)}, \tag{29}$$

where $f = u, v, w, \omega_x, \omega_y, \omega_z, \theta, a, b, c, d, e, f, g$; $F_k = U_k, V_k, W_k, \Omega_{x_k}, \Omega_{y_k}, \Omega_{z_k}, \Theta_{z_k}, A_k, B_k, C_k, D_k, E_k, F_k, G_k$; and β_k is the spanwise wavenumber given by $\beta_k = 2\pi k/\lambda_z$, and λ_z is the spanwise wavelength of the fundamental spanwise Fourier mode, and $i = \sqrt{-1}$.

ISSN 2176-5480

Substituting the Fourier transforms (Eq. 29) in the vorticity transport equations (15 – 17), in the velocity Poisson equations (18 – 20), and in the heat transfer transport equation (21) yield the governing equations in the Fourier space:

$$\frac{\partial \Omega_{x_k}}{\partial t} + \frac{\partial A_k}{\partial y} - \beta_k B_k - \frac{Go^2}{\sqrt{Re}}\beta_k(D_k^2) = \frac{1}{Re}\nabla_k^2 \Omega_{x_k}, \tag{30}$$

$$\frac{\partial \Omega_{y_k}}{\partial t} + \beta_k C_k - \frac{\partial A_k}{\partial x} = \frac{1}{Re}\nabla_k^2 \Omega_{y_k}, \tag{31}$$

$$\frac{\partial \Omega_{z_k}}{\partial t} + \frac{\partial B_k}{\partial x} + \frac{\partial C_k}{\partial y} - \frac{Go^2}{\sqrt{Re}}\frac{\partial (D_k^2)}{\partial x} = \frac{1}{Re}\nabla_k^2 \Omega_{z_k}, \tag{32}$$

$$\frac{\partial^2 U_k}{\partial x^2} - \beta_k^2 U_k = -\beta_k \Omega_{y_k} - \frac{\partial^2 V_k}{\partial x \partial y}, \tag{33}$$

$$\frac{\partial^2 V_k}{\partial x^2} + \frac{\partial^2 V_k}{\partial y^2} - \beta_k^2 V_k = -\frac{\partial \Omega_{z_k}}{\partial x} + \beta_k \Omega_{x_k}, \tag{34}$$

$$\frac{\partial^2 W_k}{\partial x^2} - \beta_k^2 W_k = \frac{\partial \Omega_{y_k}}{\partial x} + \beta_k \frac{\partial V_k}{\partial y}, \tag{35}$$

$$\frac{\partial \Theta_k}{\partial t} + \frac{\partial E_k}{\partial x} + \frac{\partial F_k}{\partial y} - i\beta_k G = \frac{1}{Re\ Pr}\nabla_k^2 \Theta_k, \tag{36}$$

where $\nabla_k^2 = \left(\frac{\partial^2}{\partial x^2} + \frac{\partial^2}{\partial y^2} - u^2\beta^2\right)$.

The equations (30 – 36) were solved numerically in the domain shown schematically in Fig. 1. The calculations are done on an orthogonal uniform grid, parallel to the wall. The fluid enters the computational domain at $x = x_0$ and exits at the outflow boundary ($x = x_{max}$). Disturbances were introduced into the flow field using spanwise suction and blowing in a disturbance strip at the wall. This strip is located between x_1 and x_2. In the region located between x_3 and x_4 a buffer domain technique (Kloker *et al.*, 1993) was implemented in order to avoid wave reflections at the outflow boundary. In these simulations a 2D Navier-Stokes solution, was used as the base flow, and for the thermal boundary layer, the standard similarity solution obtained using the Pohlhausen formula was used.

The time derivatives in the vorticity transport equations were discretized with a classical 4^{th} order Runge-Kutta integration scheme (Ferziger and Peric, 1997). The spatial derivatives were calculated using a 6^{th} order compact finite difference-scheme (Souza *et al.*, 2005; Souza, 2003; Lele, 1992). The V-Poisson equation – Eq. (34) – was solved using a multigrid Full Approximation Scheme (FAS) (Stuben and Trottenberg, 1981). A V-cycle working with 4 grids was implemented.

3.2 Boundary Conditions

The governing equations are complemented by the specification of boundary conditions. At the wall ($y = 0$), a no-slip condition was imposed for the streamwise (U_k) and the spanwise (W_k) velocity components. The wall-normal velocity component at the wall (V_k) was specified at the suction and blowing strip region between x_1 and x_2, where the disturbances were introduced. Away from the disturbance generator this velocity component was set to zero. The function used for the wall-normal velocity $V_{k=1}$ at the disturbance generator is:

$$\begin{aligned} V_{k=1}(i,0,t) &= A\sin^3(\epsilon) \quad \text{for} \quad l_1 \le i \le l_2 \quad \text{and} \\ V_{k=1}(x,0,t) &= 0 \quad \text{for} \quad l < l_1 \quad \text{and} \quad l > l_2, \end{aligned} \tag{37}$$

where $\epsilon = (l - l_1)/(l_2 - l_1)$ and A is a real constant chosen to adjust the amplitude of the disturbance. The variable l indicates the grid point location x_l in the streamwise direction, and points l_1 and l_2 correspond to x_1 and x_2 respectively. For all modes $k \neq 1$ the value of $V_k = 0$ at the wall was settled.

At the inflow boundary ($x = x_0$), the velocity, the vorticity components and the temperature are specified based on the similarity solutions. At the outflow boundary ($x = x_{max}$), the second derivatives with respect to the streamwise direction of the velocity and vorticity components are set to zero. At the upper boundary ($y = y_{max}$) the flow is considered non

ISSN 2176-5480

rotational. This is satisfied by setting all vorticity components and their derivatives to zero. The wall-normal velocity component at the upper boundary was settled according to the condition:

$$\left.\frac{\partial V_k}{\partial y}\right|_{x,y_{max},t} = 0. \tag{38}$$

This condition was imposed in the solution of the U_k velocity in the Poisson equation (Eq.33). The equations used for evaluating the vorticity components at the wall are:

$$\frac{\partial^2 \Omega_{x_k}}{\partial x^2} - \beta_k^2 \Omega_{x_k} = -\frac{\partial^2 \Omega_{y_k}}{\partial x \partial y} - \beta_k \nabla_k^2 V_k \tag{39}$$

$$\frac{\partial \Omega_{z_k}}{\partial x} = \beta_k \Omega_{x_k} - \nabla_k^2 V_k. \tag{40}$$

A damping zone near the outflow boundary was defined in which all the disturbances are gradually damped down to zero (Kloker *et al.*, 1993). This technique is used to avoid reflections in the outflow boundary. Meitz and Fasel (2000) adopted a fifth order polynomial, and the same function was used in the present code. The basic idea is to multiply the vorticity components by a ramp function $f_1(x)$ after each sub-step of the integration method. Using this technique, the vorticity components are taken as:

$$\Omega_k(x, y, t) = f_1(x)\Omega_k^*(x, y, t), \tag{41}$$

where $\Omega_k^*(x, y, t)$ is the disturbance vorticity component that results from the Runge-Kutta integration and $f_1(x)$ is a ramp function that goes smoothly from 1 to 0. The implemented function was:

$$f_1(x) = f(\epsilon) = 1 - 6\epsilon^5 + 15\epsilon^4 - 10\epsilon^3, \tag{42}$$

where $\epsilon = (l - l_3)/(l_4 - l_3)$ for $l_3 \leq l \leq l_4$. The points l_3 and l_4 correspond to the positions x_3 and x_4 in the streamwise direction, respectively. To ensure good numerical results a minimum distance between x_3 and x_4 and between x_4 and the end of the domain x_{max} has to be adopted. In the simulations presented here each zone had 30 grid points.

Another buffer domain, located near the inflow boundary was also implemented in the code. As pointed out by Meitz (1996), in simulations involving streamwise vortices, reflections due to the vortices at the inflow can contaminate the numerical solution. The damping function is similar to the one used for the outflow boundary:

$$f_2(x) = f(\epsilon) = 6\epsilon^5 - 15\epsilon^4 + 10\epsilon^3, \tag{43}$$

where ϵ is $\epsilon = (l - 1)/(l_1 - 1)$ for the range $1 \leq l \leq l_1$. All the vorticity components were multiplied by this function in this region.

The boundary conditions for the temperature were:

- inflow – $\theta = 0$;
- outflow – $\theta = 0$, since the same buffer domain for the vorticity was also applied for the temperature;
- wall – $\theta = 0$;
- upper boundary – the values were obtained from the heat transfer transport equation.

4. Results

The parameters adopted in the simulations were: the Reynolds number was Re = 10000; the Goertler number was Go = 2.385; the free stream velocity was $U_\infty = 3m/s$ the distance between two consecutive points in the x and y directions were dx = 0.015 and dy = 0.0006; the Prandtl number was Pr = 0.72; the number of points in the x and y directions were 857, and 561, respectively; the time step was dt = 0.003; the disturbances were introduced in the region $1.735 \leq x \leq 2.185$, with an amplitude of A = 0.005; in the z direction, 21 Fourier modes were used with 64 points in the physical space. The disturbances were introduced for six different spanwise wavelengths: $\lambda_z = 0.05, \lambda_z = 0.10, \lambda_z = 0.15, \lambda_z = 0.20, \lambda_z = 0.25$ and $\lambda_z = 0.30$.

The heat transfer analysis is carried out by verifying the evolution of the spanwise–average Stanton number in the streamwise direction. The Stanton number is given by:

$$St_x = \frac{Nu_x}{PrRe_x}, \tag{44}$$

ISSN 2176-5480

where Nu_x is the Nusselt number:

$$Nu_x = q_{wall}\frac{L}{k(T_e - T_w)}, \tag{45}$$

where q_{wall} is the heat flux at the wall:

$$q_{wall} = -k\frac{\partial T}{\partial y}\bigg|_{wall} \tag{46}$$

The energy is also analyzed, and for each Fourier spanwise mode it is calculated by:

$$E_k = \int_0^\infty (|U_k|^2 + |V_k|^2 + |W_k|^2)dy \tag{47}$$

for $k > 0$, and

$$E_k = \frac{1}{2}\int_0^\infty (|U_k|^2 + |V_k|^2)dy \tag{48}$$

for $k = 0$

In this calculation only the disturbance components are taken into account (Lee and Liu, 1992).

It should be emphasized that all results presented here were obtained with the introduction of steady disturbances, therefore the secondary instability was not studied in the present paper.

4.1 Results for λ_z = 0.05

The vortices are amplified initially in a linear manner and downstream when the amplitude of then is already high in the non-linear region of their development, there is the formation of mushroom-like structure with a distribution of the velocity component in the main flow direction.

Figure 2 shows energy distribution in the streamwise direction for the steady modes from 1 to 10, and also the mean flow mode (0). Between the Re_x equal 2.5×10^4 until 1.0×10^5 the Goertler vortices show a linear growth. After Re_x = 1.0×10^5, the vortices saturates and almost all modes remains with constant amplitude. In the saturation region the difference between the amplitude of consecutive modes are almost constant, and the amplitudes of the last modes are very small.

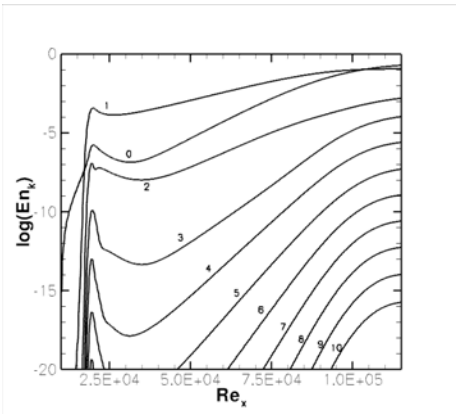

Figure 2: Energy distribution for each mode in the streamwise direction for $\lambda_z = 0.05$.

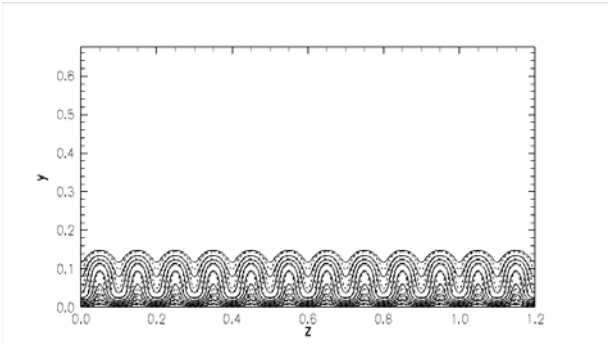

Figure 3: $\widetilde{u}$ isovelocity contours in the zy-plane at $Re_x \sim 3.32 \times 10^5$ for $\lambda_z = 0.05$.

Figure 3 shows the isovelocity and isotemperature distribution in a crosscut at Re_x = 3.32×10^5. The hydrodynamic boundary layer is shown with dashed lines and the thermal boundary layer is shown with solid lines. Since the simulations were carried out for $Pr = 0.72$ the thermal boundary layer is higher than the hydrodynamic boundary layer. The downwash region is more pronounced than the upwash region giving a higher spanwise–average heat transfer rate.

The streamwise evolution of the spanwise–average Stanton number is show in Fig. 4. The disturbance is imposed in the region at $Re_x \sim 0.6 \times 10^5$. At the beginning when the vortices are in the linear development region the curve fits the laminar flow. It can be seen that after $Re_x \sim 1.6 \times 10^5$ Goertler flow intensifies the heat transfer. Since $Re_x = 6.0 \times 10^4$ the rate of heat transfer begins to increase. At $Re_x = 1.09 \times 10^5$ the Stanton number with Goertler flow is 143% higher than laminar and and 13% lower than turbulent values respectively. The result obtained in the present case showed that with this wavelength the reached value did not reach the turbulent values predicted for turbulent flows.

ISSN 2176-5480

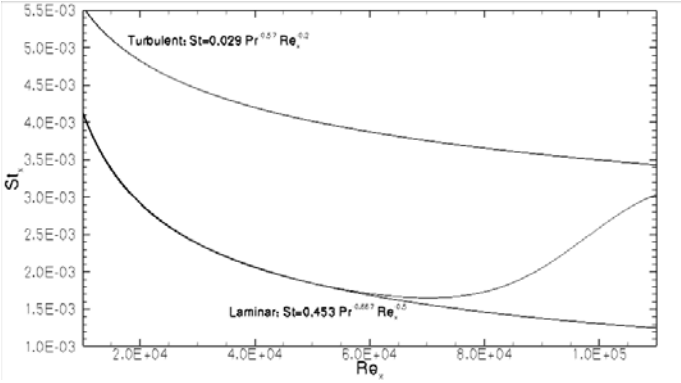

Figure 4: Streamwise evolution of the spanwise–averaged Stanton number for $\lambda_z = 0.05$.

4.2 Results for λ_z = 0.10

Figure 5 shows the energy distribution in the streamwise direction. The saturation energy obtained in the present case reached lower values than the first case (λ_z = 0.05). The saturation region starts at a streamwise position $Re_x = 8.0 \times 10^4$.

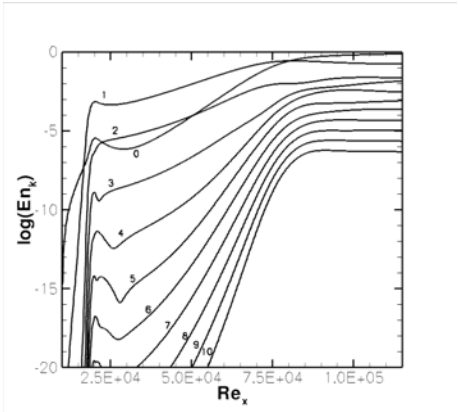

Figure 5: Energy distribution for each mode in the streamwise direction for $\lambda_z = 0.10$.

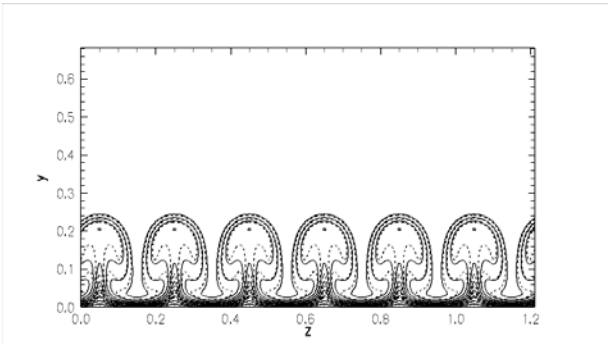

Figure 6: $\widetilde{u}$ isovelocity contours in the zy-plane at $Re_x \sim 3.32 \times 10^5$ for $\lambda_z = 0.10$.

The isovelocity and isotemperature contours for the streamwise velocity at $Re_x \sim 3.32 \times 10^5$ is shown in Fig. 6. The mushroom structure typical for Goertler flow can be seen. The velocity field of the vortice induces periodic motion nomal the transverse direction in the boundary layer, which changes when the developing regions of low momentum of the fluid moves away from the wall and the fluid at high speed moves to the outer wall. In this figure it can be more pronounced than the upwash region. This helps for understand that the spanwise–average Stanton number increases in the nonlinear development region.

Figure 7 shows the streamwise evolution of the spanwise–average Stanton number for $\lambda_z = 0.10$. It can be seen that after $Re_x \sim 1.8 \times 10^5$, the Goertler flow intensifies the heat transfer. At $Re_x = 1.09 \times 10^5$ the The Stanton number with Goertler flow is 299% and 45% higher than laminar and turbulent values respectively. In this case we have the biggest gain for the rate of heat transfer of all simulated cases.

4.3 Results for λ_z = 0.15

Figure 8 shows the energy distribution for each mode from 0 to 10 for λ_z = 0.15. The saturation region starts at a streamwise position $Re_x = 8.0 \times 10^4$, almost at the same position observed for λ_z = 0.10.

The isovelocity and isotemperature distribution in a crosscut at $Re_x \sim 3.32 \times 10^5$ is shown in Fig. 9.

Figure 10 shows the streamwise evolution often the Stanton number for λ_z = 0.15. In the present case at $Re_x = 1.09 \times 10^5$ the Stanton number with Goertler flow reaches 234% and 22% higher than laminar and turbulent values respectively.

4.4 Results for λ_z = 0.20

Figure 11 shows energy distribution in the streamwise direction for the steady modes from 1 to 10, and also the mean flow mode (0). The saturation region starts at a streamwise position $Re_x = 8.0 \times 10^4$, almost at the same position

ISSN 2176-5480

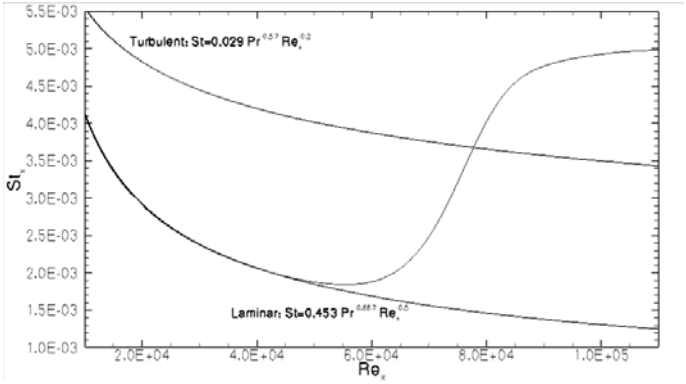

Figure 7: Streamwise evolution of the spanwise–averaged Stanton number for $\lambda_z = 0.10$.

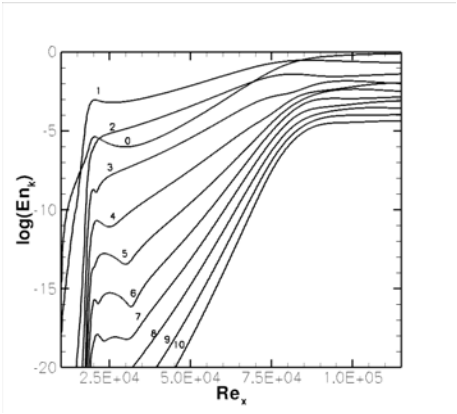

Figure 8: Energy distribution for each mode in the streamwise direction for $\lambda_z = 0.15$.

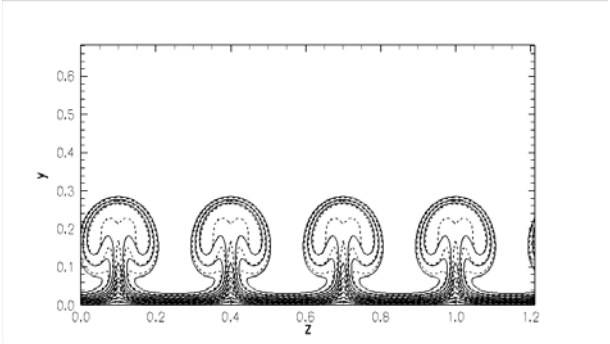

Figure 9: $\widetilde{u}$ isovelocity contours in the zy-plane at $Re_x \sim 3.32 \times 10^5$ for $\lambda_z = 0.15$.

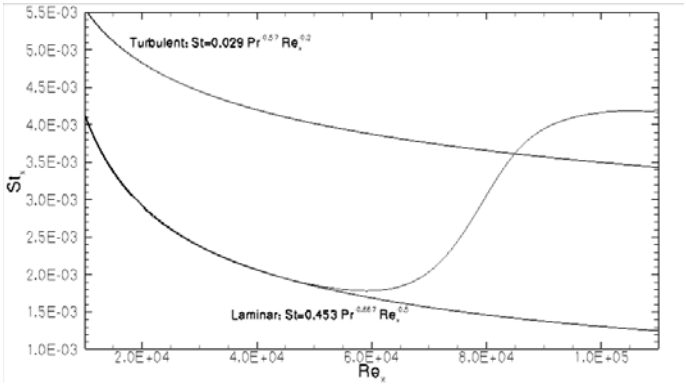

Figure 10: Streamwise evolution of the spanwise–averaged Stanton number for $\lambda_z = 0.15$.

observed for λ_z = 0.10 and λ_z = 0.15.

The isovelocity and isotemperature contours for the streamwise velocity at $Re_x \sim 3.32 \times 10^5$ is shown in Fig. 12.

Figure 13 shows the streamwise evolution of the Stanton number for λ_z = 0.20. In the present case at $Re_x = 1.09 \times 10^5$ the Stanton number with Goertler flow is 173% higher than laminar and 0.1% lower than turbulent values, respectively. These results show that the growth of the vortices were not monotonic.

4.5 Results for λ_z = 0.25

Figure 14 shows energy distribution in the streamwise direction for the steady modes from 1 to 10, and also the mean flow mode (0). The saturation region starts at a streamwise position $Re_x = 5.0 \times 10^4$.

The isovelocity and isotemperature contours for the streamwise velocity at $Re_x \sim 3.32 \times 10^5$ is shown in Fig. 15.

Figure 16 shows the streamwise evolution often the Stanton number for λ_z = 0.25. In the present case at $Re_x = 1.09 \times 10^5$ the Stanton number with Goertler flow reaches 238% and 23% higher than laminar and turbulent values respectively. This case has the second best result for the gain in heat transfer and shows that the growth of the vortices

ISSN 2176-5480

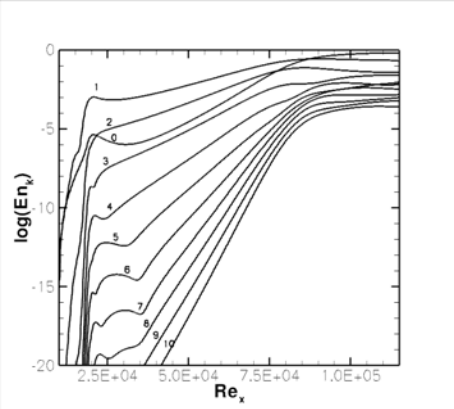

Figure 11: Energy distribution for each mode in the streamwise direction for $\lambda_z = 0.20$.

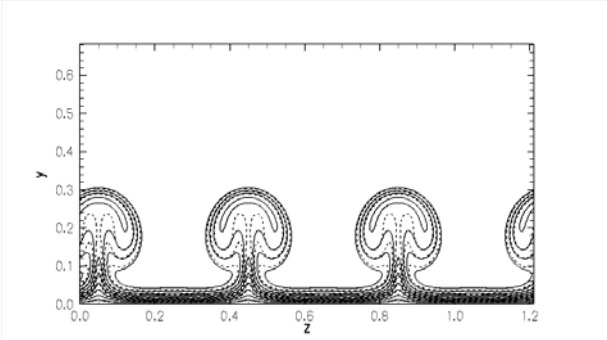

Figure 12: $\widetilde{u}$ isovelocity contours in the zy-plane at $Re_x \sim 3.32 \times 10^5$ for $\lambda_z = 0.20$.

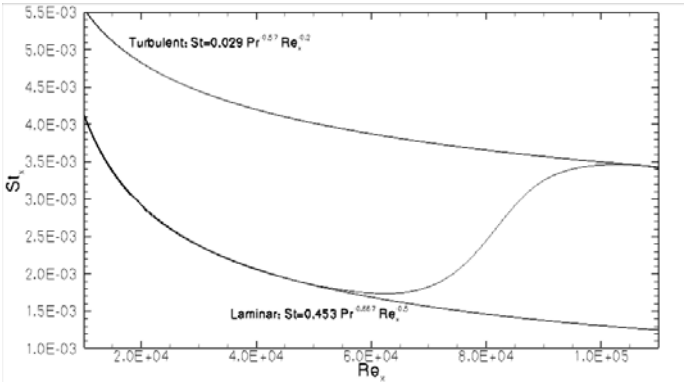

Figure 13: Streamwise evolution of the spanwise–averaged Stanton number for $\lambda_z = 0.20$.

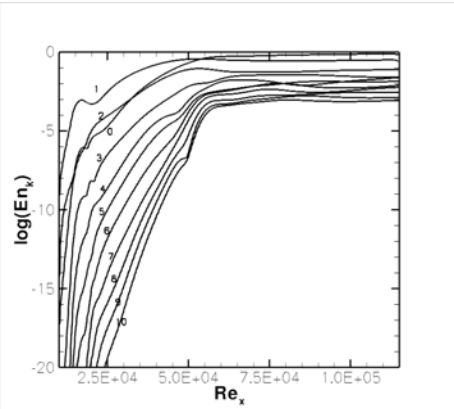

Figure 14: Energy distribution for each mode in the streamwise direction for $\lambda_z = 0.25$.

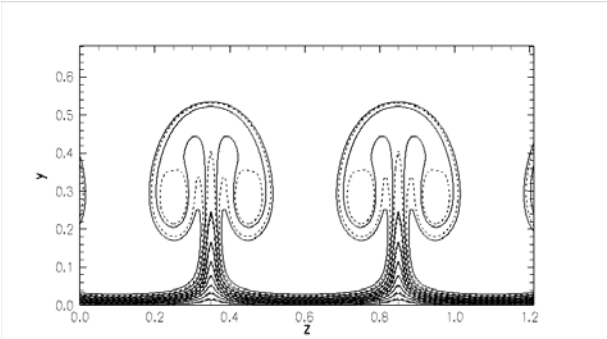

Figure 15: $\widetilde{u}$ isovelocity contours in the zy-plane at $Re_x \sim 3.32 \times 10^5$ for $\lambda_z = 0.25$.

were not monotonic.

4.6 Results for λ_z = 0.30

Figure 17 shows energy distribution in the streamwise direction for the steady modes from 1 to 10, and also the mean flow mode (0). The saturation region starts at a streamwise position $Re_x = 6.0 \times 10^4$.

The isovelocity and isotemperature contours for the streamwise velocity at $Re_x \sim 3.32 \times 10^5$ is shown in Fig. 18.

Figure 19 shows the streamwise evolution often the Stanton number for λ_z = 0.30. In the present case at $Re_x = 1.09 \times 10^5$ the Stanton number with Goertler flow reaches 207% and 22% higher than laminar and turbulent values respectively.

ISSN 2176-5480

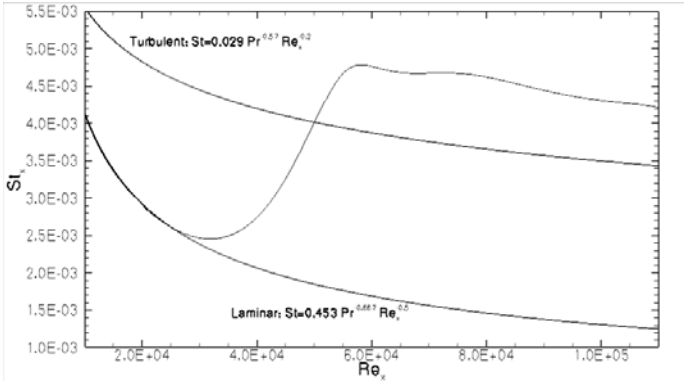

Figure 16: Streamwise evolution of the spanwise–averaged Stanton number for $\lambda_z = 0.25$.

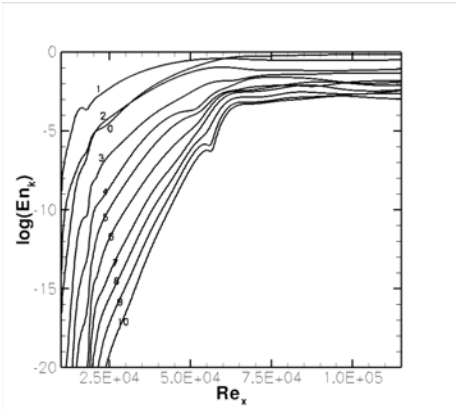

Figure 17: Energy distribution for each mode in the streamwise direction for $\lambda_z = 0.30$.

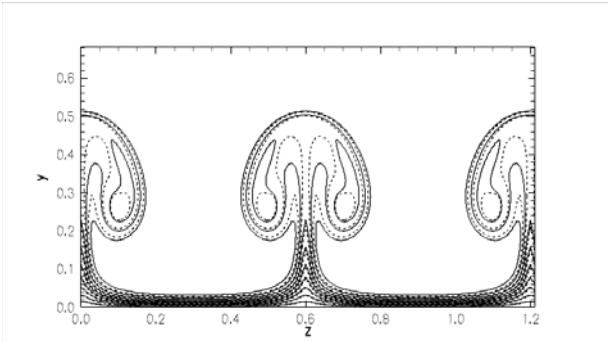

Figure 18: $\widetilde{u}$ isovelocity contours in the zy-plane at $Re_x \sim 3.32 \times 10^5$ for $\lambda_z = 0.30$.

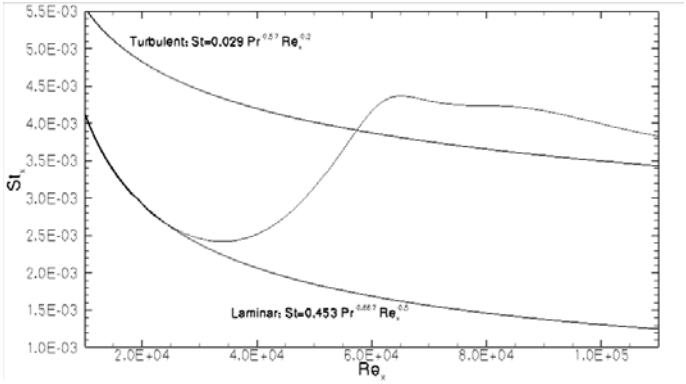

Figure 19: Streamwise evolution of the spanwise–averaged Stanton number for $\lambda_z = 0.30$.

5. Conclusion

In the present paper it was analysed the influence of the spanwise wavelengths: λ_z = 0.05, λ_z = 0.10, λ_z = 0.15, λ_z = 0.20, λ_z = 0.25 and λ_z = 0.30 for $Pr = 0.72$, in the heat transfer rate. Although the secondary instability was not studied, it was observed that the steady Goertler flow can reach heat transfer rates higher than the turbulent boundary layes flows. Although some authors believe that the high heat transfer rates is a consequence of Goertler flow secondary instabilities, with the present results one can see that the Goertler flow itself is responsible to achieve these gains. Comparing the six spanwise wavelengths results, it was observed that for λ_z = 0.10 the higher gain in heat transfer rate was observed, and in 5 of the 6 cases studied that the Stanton number reached values higher than the turbulent ones. It was observed also that this gain is not monotonic with the spanwise wavelength.

6. ACKNOWLEDGEMENTS

The authors acknowledge the financial support received from FAPESP under Grant No. 2010/00495-1.

ISSN 2176-5480

7. REFERENCES

Ferziger, J.H. and Peric, M., 1997. *Computational Methods for Fluid Dynamics*. Springer-Verlag Berlin Heidelberg New York.

Fiebig, M., 1996. "Vortices and heat transfer". *Zeitschrift fur Angewandte Mathematik und Mechanik*, Vol. 76, pp. 1–16.

Floryan, J.M. and Saric, W.S., 1982. "Stability of Görtler vortices in boundary layers". *AIAA Journal*, Vol. 20, pp. 316–324.

Girgis, I.G. and Liu, J.T.C., 2006. "Nonlinear mechanics of wavy instability of steady longitudinal vortices and its effect on skin friction rise in boundary layer flow". *Physics of Fluids*, Vol. 18.

Kloker, M., Konselmann, U. and Fasel, H., 1993. "Outflow boundary conditions for spatial navier-stokes simulations of transition boundary layer". *AIAA Journal*, Vol. 31, pp. 620–628.

Lee, K. and Liu, J.T.C., 1992. "On the growth of the mushrromlike structures in nonlinear spatially developing Görtler vortex flow". *Physics of Fluids*, Vol. A4, pp. 95–103.

Lele, S.K., 1992. "Compact finite difference schemes with spectral-like resolution". *Journal of Computational Physics*, Vol. 103, pp. 16–42.

Liu, J.T.C., 2008. "Nonlinear instability of developing streamwise vortices with applications to boundary layer heat transfer intensification thought an extended reynolds analogy". *Philosophical Transactions of the Royal Society*, Vol. 366, pp. 101–112.

Liu, J.T.C. and Lee, K., 1995. "Heat transfer in a strongly nonlinear spatially developing longitudinal vorticity system". *Physics of Fluids*, Vol. 7, pp. 559–599.

Meitz, H.L., 1996. *Numerical Investigation of Suction in a Trasition Flat-Plate Boundary Layer*. Ph.D. thesis, The University of Arizona.

Meitz, H. and Fasel, H., 2000. "A compact-difference scheme for the navier-stokes equations in vorticity-velocity formulation". *Journal of Computational Physics*, Vol. 157, pp. 371–403.

Mitsudharmadi, H., Winoto, S.H. and Shah, D.A., 2004. "Development of boundary-layer flow in the presence of forced wavelength goertler vortices". *Physics of Fluids*, Vol. 16.

Momayez, L., Dupont, P., Delacourt, G., Lottin, O. and Peershossaini, H., 2009. "Genetic algorithm based correlations for heat transfer calculation on concave surfaces". *Applied Thermal Engineering*, Vol. 29, pp. 3476–3481.

Momayez, L., Dupont, P. and Peershossaini, H., 2004. "Effects of vortex organization on heat transfer enhancement by goertler instability". *International Journal of Thermal Sciences*, Vol. 43, pp. 753–760.

Momayez, L. and Peershossaini, H., 2004. "Some unexpected effects of wavelenght and pertubation strength on heat transfer enhancement by Görtler instability". *International Journal of Heat and Mass Transfer*, Vol. 47, pp. 495–492.

Peerhossaini, H., 1987. *L'Instabilite d'une couche limite sur une paroi concave (les tourbilons de Görtler.* Ph.D. thesis, Univ. Pierre et Marie Curie, Paris.

Saffmann, P.G., 1992. *Vortex Dynamics*. Cambridge University Press.

Souza, L.F., 2003. *Instabilidade Centrífuga e Transição para Turbulência em Escoamentos Laminares sobre Superfícies Côncavas*. Ph.D. thesis, Instituto Tecnológico de Aeronáutica, Brazil.

Souza, L.F., Mendonça, M.T. and Medeiros, M., 2005. "The advantages of using high-order finite differences schemes in laminar-turbulent transition studies". *International Journal for Numerical Methods in Fluids*, Vol. 48, pp. 565–592.

Stuben, K. and Trottenberg, U., 1981. *Nonlinear Multigrid Methods, the Full Approximation Scheme*. Koln-Porz.

Swearingen, J. and Blackwelder, R., 1987. "The growth and breakdown of streamwise vortices in the presence of a wall". *Journal of Fluid Mechanics*, Vol. 182, pp. 255–290.

Tandiano, Winoto, S.H. and Shah, D.A., 2009. "Wall shear stress in goertler sortex boundary layer flow". *Physics of Fluids*, Vol. 21.

8. RESPONSIBILITY NOTICE

The authors are the only responsible for the printed material included in this paper.